Nanostructures

DOI: 10.1002/ange.200501361

Synthesis of Semiconducting Thin Films with Nanometer-Scale Periodicity by Solution-Phase Coassembly of Zintl Clusters with Surfactants**

*Andrew E. Riley, Scott D. Korlann, Erik K. Richman, and Sarah H. Tolbert**

The cooperative self-assembly of inorganic precursors with organic surfactants or polymeric structure-directing agents has led to the synthesis of many oxide-based, nanostructured composite materials that show periodicity. Oxide powders, monoliths, and thin films with a diverse range of compositions (TiO_2, ZrO_2, Nb_2O_5, SnO_2, Mn_xO_y, Al_2O_3, and others) have been prepared following the work on surfactant-templated silicas (MCM-41-type materials).[1–17] Although the powdered forms of these materials have many proposed uses, including catalysis and size-selective separation, the thin-film forms have significantly expanded their potential.[18–23] The thin-film morphology has several applications for which bulk materials are not useful, including low-k dielectric coatings, optical waveguides, and membranes.[24–27]

Despite the many exciting potential applications of these periodic surfactant-templated thin films, there are still significant limitations to oxide-based materials. The most significant of these limitations is that most oxides are insulators, or wide-band-gap semiconductors, which limits their use in applications based on electrical conductivity because of their high intrinsic resistance and low carrier densities.

The development of self-assembled inorganic/organic composites based on non-oxide precursors has led to the synthesis of a variety of semiconducting composites with nanoscale periodicity.[28–36] These composite materials use highly reduced soluble metal clusters, or Zintl clusters, as an inorganic building block. The Zintl clusters can self-assemble with organic structure-directing agents in solution with the help of transition-metal cross-linkers. The resulting material is a highly periodic inorganic alloy with ordering similar to liquid-crystalline systems. These materials, which were initially designed to be analogues of silica and other oxide composites, have an advantage over most oxide systems for optoelectronic applications in that their range of band gaps can be tuned between 0.6 and 3.4 eV depending on their chemical composition.[28–37] Unfortunately, although composites with a wide range of electronic properties have been synthesized, their macroscale morphology has been limited to bulk powders, thus restricting their usefulness in some applications.

As with the oxide materials mentioned previously, knowledge of the macroscale morphology of this class of non-oxide materials helps to determine the optimal applications of the composites. Many of the proposed applications for the non-oxide composite materials, such as photovoltaics, ambipolar field-effect transistors (FETs), and chemical sensing, rely on the electrical conductivity of the composite. Bulk powders present several problems for the effective assembly of an electronic device, most notably the contact resistance between the powder and the electrode as well as between grains within the powder. A thin-film morphology should be able to overcome these obstacles if the film can be grown in intimate contact with a substrate that can double as an electrical contact.

To address this fundamental need, we report here the synthesis of semiconducting non-oxide thin films with a variety of compositions and structures by coassembly of Zintl clusters with cationic surfactants. Interestingly, in some cases, thin films form with phases that have not been observed in bulk composite powders. The phases formed range in nanoscale architecture from a partly disordered wormlike phase, to a periodic, hexagonal, honeycomb structure, and on to a highly ordered cubic geometry. The surface-nucleated growth mechanism used to synthesize these thin films appears to stabilize both new compositions and phases that are otherwise inaccessible in these systems. Furthermore, our results indicate that the optical homogeneity of the films can be modified by adding reagents that chelate the cross-linking transition metal. Layered thin films can also be synthesized in the absence of a metal cross-linking agent. UV/Vis/NIR reflectance data indicate that materials with a broad range of band gaps can be created. Finally, as expected for a semiconducting thin film, diode characteristics are observed in the current–voltage measurements when asymmetric electrodes are employed.

The solution-phase self-assembly of these non-oxide thin films was carried out under inert conditions. The Zintl cluster, a surfactant (cetyltriethylammonium bromide), and the transition-metal salt were all dissolved in formamide. A gold substrate was then placed in contact with the solution such that the gold was inverted to prevent sedimentation on the surface. This mixture was held at 60 °C for one hour during which time the films grew on the surface. Profilometry indicates that films could be formed with a range of thicknesses. The data indicate that films ranging from 90 to about 500 nm thick could be produced, depending on the reactivity of the cross-linking metal, the growth time of film, and the surfactant concentration. Films could also be prepared without a transition-metal cross-linking agent by taking advantage of the self-oligomerization of tin telluride ($SnTe_4^{4-}$). Such films were synthesized in a similar manner, although in this case room temperature and a growth time of 8 hours were employed.

Figure 1 shows typical low-angle X-ray diffraction patterns for thin films of five different phases and compositions.

[*] Dr. A. E. Riley, S. D. Korlann, E. K. Richman, Prof. S. H. Tolbert
Department of Chemistry and Biochemistry
The University of California, Los Angeles
Los Angeles, CA 90095-1569 (USA)
Fax: (+1) 310-206-4038
E-mail: tolbert@chem.ucla.edu

[**] This work was supported by the National Science Foundation under grant CHE-9985259 and by the Office of Naval Research under grant N00014-04-1-0410. S.H.T. is an Alfred P. Sloan Foundation Research Fellow.

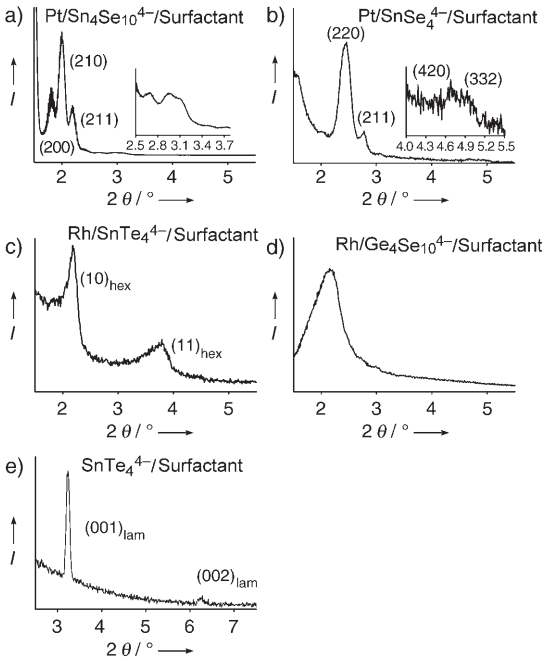

Figure 1. Low-angle X-ray diffraction patterns of nanostructured semiconducting inorganic/surfactant composite thin films: a) a thin film synthesized using Pt-coupled $Sn_4Se_{10}^{4-}$ clusters demonstrates a cubic *Pm*3*n* morphology (peak-position ratio $1:\sqrt{5}/2:\sqrt{6}/2$); b) a thin film synthesized using Pt-coupled $SnSe_4^{4-}$ clusters demonstrates a cubic *Ia*3*d* morphology (peak-position ratio $1:\sqrt{8}/\sqrt{6}:\sqrt{4}/\sqrt{6}:\sqrt{20}/\sqrt{6}$); c) a thin film synthesized from Rh-coupled $SnTe_4^{4-}$ clusters has a 2D hexagonal *P*6*mm* morphology (peak position ratio $1:\sqrt{3}$); d) a thin film synthesized from Rh-coupled $Ge_4Se_{10}^{4-}$ clusters has a disordered, probably wormlike geometry; e) a thin film synthesized by the self-oligomerization of $SnTe_4^{4-}$ clusters in the presence of surfactant has a layered lamellar structure.

The labels for each composite are based on the precursors used to synthesize the films, and are not indicative of the exact final stoichiometry of the films. In Figure 1a, a Pt-coupled $Sn_4Se_{10}^{4-}$/surfactant composite shows the (200), (210), and (211) diffraction peaks of a cubic *Pm*3*n* architecture.[38] The bulk analogue of this system has been shown to form either a 2D hexagonal (*P*6*mm*) or a cubic (*Ia*3*d*) phase.[30] The formation of a thin film with a periodicity different from those of the bulk analogues demonstrates the importance of surface stabilization to the nanoscale architecture. Figure 1b shows the (211), (220), (420), and (332) diffraction pattern of a cubic *Ia*3*d* phase of a Pt-coupled $SnSe_4^{4-}$/surfactant composite. While *Ia*3*d* phases have been observed previously in related bulk composites based on Zintl clusters,[30] this phase has not been observed previously for any nanostructured thin film, including silica-based composite thin films.[18–22] The absence of this phase likely stems from the fact that a flat substrate does not provide a good interfacial nucleation site for the *Ia*3*d* phase. The observation of this phase for Zintl cluster based systems suggests that the nucleation process is fundamentally different in these materials compared to oxide-based systems. This point will be discussed further below.

Figure 1c shows the low-angle diffraction pattern for a Rh-coupled $SnTe_4^{4-}$/surfactant composite thin film. This composite has a 2D hexagonal (*P*6*mm*) architecture as evidenced by the (10) and (11) peaks of this phase with a position ratio of $1:\sqrt{3}$. This material has a unit-cell parameter *a* of 46.1 Å. This repeat distance is slightly larger than the distances that have been observed in bulk composites of similar composition. A direct comparison of the structure with a bulk system, however, can not be made because the Rh/$SnTe_4^{4-}$/surfactant system has not been successfully synthesized as a bulk nanostructured composite. The presence of both a fundamental $(10)_{hex}$ and a $(11)_{hex}$ reflection indicates that although the film does have hexagonal order it is not constrained to the plane of the substrate, which would be lead to an absence of the $(11)_{hex}$ reflection in a θ–θ diffraction geometry. Low-angle X-ray diffraction studies on the bulk precipitate (not shown) indicate that the corresponding bulk system has no such structure. The lack of structure in the bulk precipitate again emphasizes the fact that the surface-growth mechanism allows the synthesis of composite films whose compositions are not accessible in powder form.

Figure 1d shows the low-angle X-ray diffraction pattern for a Rh-coupled $Ge_4Se_{10}^{4-}$/surfactant composite thin film. This film exhibits only one peak, which is indicative of a phase with a characteristic repeat distance, but no long-range order. This wormlike phase has a fundamental repeat distance of 42 Å. Finally, Figure 1e shows the diffraction pattern for a thin film prepared through Zintl-cluster auto-oligomerization without a transition-metal cross-linking agent. The $SnTe_4^{4-}$/surfactant composite has the (001) and (002) peaks at a 1:2 position ratio which would be expected for a layered composite.

Table 1 is a summary of the various compositions of thin films that have been synthesized thus far. Whereas in some cases, such as in the Rh/$SnTe_4^{4-}$/surfactant and Pt/$Sn_4Se_{10}^{4-}$/surfactant films described above, the films demonstrate hexagonal or cubic order, in many cases the films demonstrate a more disordered "wormlike" structure similar to that observed in Figure 1d. Such a single peak can be observed even for materials in which long range periodicity is not present. The position of these single peaks ranges from 34 to 43 Å for the wormlike structures. Hexagonal materials exhibit similar fundamental peak positions in the range between 38 and 42 Å. These peak positions correspond to hexagonal unit-cell parameters *a* that range from 44 to 49 Å. These values are reasonable compared to those of powders of non-oxide hexagonal composite systems prepared with similar surfactants.[28] The agreement between the patterns of the hexagonal and wormlike materials further emphasizes the fact that the disordered materials are likely to be composed of randomly assembled cylindrical micelles. The cubic *Pm*3*n* Pt/$Sn_4Se_{10}^{4-}$/surfactant composite has a unit-cell parameter *a* of 98 Å, whereas the cubic *Ia*3*d* Pt/$SnSe_4^{4-}$/surfactant composite has a unit-cell parameter *a* of 86 Å. Both of these values are in reasonable agreement with those of analogous silica-based cubic structures.[2,39] Finally, the lamellar $SnTe_4^{4-}$/surfactant system has a layer spacing of 28 Å, a value which has been observed previously for layered phases formed with cetyltriethylammonium bromide.[2]

Table 1 also includes the elemental data obtained from energy-dispersive spectroscopy (EDS) for the majority of

Table 1: Summary of the compositions, phases, and average fundamental repeat distances of the thin film composites.

Composite[a]	Unit-cell parameter *a* [Å][b]	Bulk analogue[c]	Elemental analysis[d]
wormlike			
$Rh/Ge_4Se_{10}^{4-}$	42	no	
$Pt/Ge_4Se_{10}^{4-}$	35	yes	$Pt_{0.8}Ge_4Se_{10.4}$
$Pd/Sn_4Se_{10}^{4-}$	41	no	$Pd_{0.9}Sn_4Se_{12.6}$
$Ni/Sn_4Se_{10}^{4-}$	40	no	$Ni_{1.4}Sn_4Se_{12.4}$
$Rh/Sn_4Se_{10}^{4-}$	42	no	$Rh_{1.3}Sn_4Se_{11}$
$Ir/Sn_4Se_{10}^{4-}$	42	no	
$Ni/SnSe_4^{4-}$	37	no	$Ni_{1.1}SnSe_4$
$Pt/SnSe_4^{4-}$	37	no	$Pt_{1.3}SnSe_{4.6}$
$Zn/SnSe_4^{4-}$	43	yes	
$Pt/SnTe_4^{4-}$	34	no	$Pt_{1.4}SnTe_{4.2}$
hexagonal			
$Ni/Ge_4Se_{10}^{4-}$	49	yes	$Ni_{0.8}Ge_4Se_{10.4}$
$Pt/Sn_4Se_{10}^{4-}$	44	yes	$Pt_{1.3}Sn_4Se_{9.7}$
$Rh/SnTe_4^{4-}$	48	no	$Rh_{0.7}SnTe_{3.4}$
cubic Pm3n			
$Pt/Sn_4Se_{10}^{4-}$	98	no	$Pt_{1.2}Sn_4Se_{9.4}$
cubic Ia3d			
$Pt/SnSe_4^{4-}$	86	no	$Pt_{1.3}SnSe_{3.6}$
lamellar			
$SnTe_4^{4-}$	28	yes	

[a] The composites are listed according to phase, and all compositions should be assumed to include surfactant. The wormlike phases have one peak, which is indicative of a characteristic repeat distance and no long-range order. Hexagonal refers to a 2D *P6mm* hexagonal, honeycomb architecture. Lamellar is a layered phase. The diffraction patterns for all five phases are shown in Figure 1. [b] Although *a* is listed for each phase, it is however, actually just a characteristic repeat distance for the wormlike phase, rather than a unit-cell parameter. [c] This indicates if a nanostructured-powder analogue has been synthesized from the same precursors. [d] Determined by energy-dispersive spectroscopy (EDS) X-ray analysis. The ratio of cross-linking metal to precursor chalcogenide cluster in the mesostructure is approximately one in all cases. More importantly, the elemental data suggests that the initial tetrahedral or adamantine cluster is incorporated into the composite as an intact unit.

composites produced. In all cases, the 1:4 or 4:10 (Group 14 element:chalcogen) stoichiometry of the initial tetrahedral or adamantane-like clusters is preserved in the final composite. Moreover, all the materials show an approximately 1:1 transition-metal:Zintl-cluster ratio, which supports the assertion that the −4 charge on the clusters is not significantly altered during the synthesis. The results of elemental analysis provide strong evidence that the overall composition of the thin film can be simply and reproducibly tuned by merely changing the nature of the solution used in the synthesis.

Beyond controlling the nanoscale structure and elemental composition, there is also an interest in producing films that are continuous on a large scale. While most of the films described here are optically quite homogeneous, there are some synthetic combinations that lead to films that have surface inhomogeneity. This surface inhomogeneity is observed visually as islands of dark material, which appears to be bulk composite material, adhered to the surface. Although the diffraction pattern of the bulk precipitate yields no structural information, it is desirable to make the thin films as homogeneous as possible. In an effort to control the homogeneity of the product, we attempted to slow down the formation of the bulk film. This was accomplished by ligating the transition-metal cross-linking ion. For example, the addition of ethylenediamine (en) to a solution of $RhCl_3$ is accompanied by a color change as the rhodium ion is complexed by the bidentate ligand. Although the addition of $RhCl_3$ to a solution of surfactant and $SnTe_4^{4-}$ yields a precipitate immediately, the addition of $[Rh(en)_x]Cl_3$ yields no precipitate until the mixture is heated. Free Rh^{3+} ions are slowly released upon heating.

Figure 2 shows the low-angle X-ray diffraction patterns and pictures of $Rh/SnTe_4^{4-}$/surfactant thin films formed with

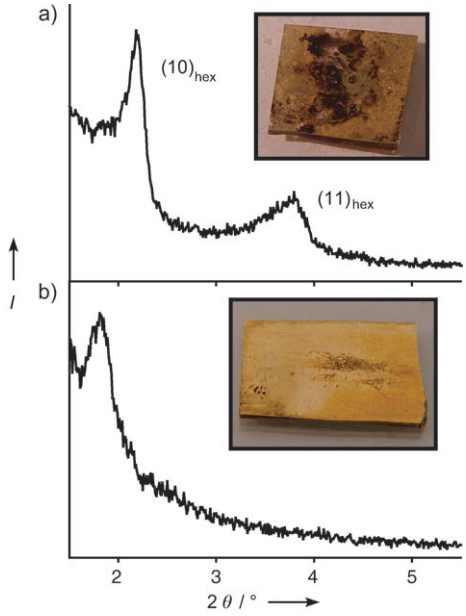

Figure 2. Low-angle diffraction patterns and pictures of $Rh/SnTe_4^{4-}$/surfactant composite thin films: a) an inhomogeneous film with hexagonal *P6mm* order (peak-position ratio $1:\sqrt{3}$); b) a film prepared by ligating the transition metal used to cross-link the structure. This film, while less ordered, is much more homogeneous.

$RhCl_3$ (Figure 2a) and $[Rh(en)_x]Cl_3$ (Figure 2b), respectively, as the Rh source. Figure 2a shows a diffraction pattern characteristic of a 2D hexagonal architecture whereas Figure 2b show a characteristic diffraction pattern of a less-ordered, wormlike structure. Also, the fundamental repeat distance of the disordered phase is 48.1 Å for this structure versus 41.5 Å for the hexagonal phase. The larger repeat distance for the en-containing phase may be indicative of a lower density of inorganic cross-links in the en-containing film or may be due to swelling of the nonpolar organic domains by en. Similarly, the lower order in the en-containing material may also be related to any reduction in the cross-linking density. Alternatively, it may be related to hydrophobic swelling by the en or more generally to the nonpolar nature of en, which is less effective than formamide at promoting amphiphilic assembly.[40,41] The insets in Figure 2, however, show that the film formed with the ligated transition

metal is much more homogeneous than the nonligated film because of the slower formation kinetics.

To understand how these films differ from oxide-based materials produced previously, some discussion of the mechanism of film formation is desirable. In bulk composites of this class of materials, the self-assembly process is the result of inorganic oligomerization coupled with electrostatic attraction to the organic surfactant. Although the surfactant generally forms multiply charged micelles in solution, the clusters initially do not associate with the micelles as a result of entropic considerations. Upon addition of a transition-metal ion, which cross-links the inorganic species, the entropic barrier to self-assembly is lowered and the composite can form. This mechanism must be different for film formation. The bulk material forms quickly because of strong electrostatic interactions, but after the bulk powder precipitates, the concentration of reactants left in solution reaches a steady state. This state is more representative of an equilibrium composition, and may even involve some dissolution of already formed powders. The thin films grow at the metal surface using the reactants that are left in solution. Confirmation of these ideas comes from cases in which the inorganic oligomerization leads to extremely rapid precipitation of the precursors—in this situation, thin films are not formed. In this case, the concentrations of the precursors remaining in solution were probably too low for appreciable film growth to take place. A similar mechanism is involved in the interface-nucleated growth of silica films from aqueous solution.[18,42]

There is, however, one distinctive difference between interface-nucleated silica films and the films presented here. For silica-based materials, the surfactant first associates with the interface and then the silica oligomers associate with the surfactant.[43,44] This process results in materials with a well-defined orientation of the nanometer-scale structure relative to that of the substrate. For example, the hexagonal *c* axis of hexagonal honeycomb-structured materials lies in the plane of the film.[18,42] For these Zintl ion based films, however, it appears that formation of the film is driven by the attraction between the Zintl cluster and the noble-metal surface, rather than by the surfactant and the surface. Contrary to the results obtained for silica-based films, this produces films that do not have a well defined orientation of the nanometer-scale structure with respect to the interface. This same effect is likely to be responsible for the fact that the *Ia3d* cubic structure, which can not produce a favorable interaction of the surfactant with the substrate, can be produced for Zintl ion based composites, even though it has not been produced in silica-based materials.

Other synthetic parameters to consider include the redox activity of the transition-metal ion used in the inorganic oligomerization. Attempts to synthesize thin films using Au^{3+} ions resulted in the gold/titanium layers delaminating from the glass, probably because of oxidation of the adherence layer by the transition-metal ion.[45] Similarly, Pd^{2+}-coupled, mesostructured films could only be produced if very short growth times were employed to minimize degradation of the metallic substrate. The Au^{3+} and Pd^{2+} ions have the largest standard reduction potentials of the transition-metal ions that were used for cross-linking, which indicates that above a certain threshold, oxidation of the substrate is a factor that needs to be considered.

Although transition-metal cross-linking is the most commonly employed method for inorganic polymerization in this class of materials, there are other means of polymerization available. One of the thin-film compositions in Table 1 and Figure 1e is synthesized without a cross-linking transition-metal ion. The formation of the tin telluride film is based on the self-oligomerization of the $SnTe_4^{4-}$ cluster.[46] Tellurium elimination condenses the cluster into larger oligomers ($Sn_2Se_7^{4-}$, $Sn_2Se_6^{4-}$), which can then self-assemble with the surfactant in an analogous manner to the model proposed above for self-assembly based on transition-metal cross-linking.[46,47]

We next consider the electronic properties of these nanoscale semiconductor thin films. The bulk analogues of these thin films are semiconductors with band gaps that range from narrow (0.6 eV) to wide (3.4 eV).[28–30,32–37] Figure 3 shows the relative absorptivity calculated from specular reflectivity data for thin films of four different compositions. The four composites show a range of band gaps from 1.1 eV ($Ir/SnSe_4^{4-}$/surfactant) to 1.5 eV ($Rh/SnTe_4^{4-}$/surfactant), as determined by Tauc plot fits to this absorptivity data.[48,49] The tunability of the band gap is believed to stem from the variable elemental composition of the composites (Table 1). Although many nanoscale semiconductors show strong quantum-confinement effects, one might expect that these amorphous semiconductors would have fairly localized excitations, which are not expected to be very sensitive to the nanometer-scale periodicity of the composite. In agreement with this idea, studies of both bulk chalcogenide glass based semiconductors and Zintl cluster based inorganic/surfactant

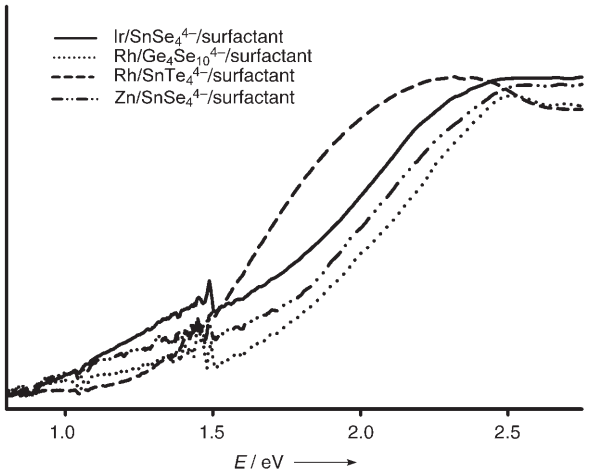

Figure 3. Relative absorptivity (α) calculated from Vis/NIR reflectance data for nanostructured, semiconducting thin films of different elemental composition. The optical band gaps of the materials were determined by using Tauc plots. All four of these materials are midgap semiconductors with band gaps of 1.1 eV ($Ir/SnSe_4^{4-}$/surfactant), 1.3 eV ($Rh/Ge_4Se_{10}^{4-}$/surfactant), 1.5 eV ($Rh/SnTe_4^{4-}$/surfactant), and 1.2 eV ($Zn/SnSe_4^{4-}$/surfactant). The noise at ca. 1.5 eV is due to a detector change in the spectrometer.

composites have shown that changes in elemental composition are primarily responsible for shifts in band gaps. This includes both changes in the transition-metal and main-group elements that make up the composite,[28–30,32–37] and changes in the stoichiometric ratios of those elements.[37,50,51] We note that depending on the exciton size in these semiconductors, there could be some quantum-confinement effects on top of this elemental tuning, but because we can not make bulk analogues with stoichiometries that are identical to these thin-film composites, such size effects can not be clearly observed.

Interestingly, examination of the data in Figure 3 shows two distinct curve shapes: concave for the Rh/$SnTe_4^{4-}$/surfactant composite and convex for the other three compositions. Concave absorption curves are expected for a direct-band-gap material, while a convex curve would be expected for an indirect-band-gap semiconductor. In agreement with this assignment, the best linear fits to the data were achieved by using the direct-band-gap form of the Tauc plot for the Rh/$SnTe_4^{4-}$/surfactant composite (E vs $E^2 \times \alpha$) and the indirect-band-gap form of the Tauc plot for the other three compositions (E vs $\sqrt{E} \times \alpha$).[48,49] In chalcogenide glasses, tellurides tend to have different electronic properties than selenides and sulfides,[52] and, in direct agreement with our reflectance data, work on tin chalcogenides shows that the telluride composite has a direct band gap whereas the selenide, sulfide, and oxide composites all have indirect band gaps.[52]

Finally, to exemplify the potential for electronic applications for these nanostructured thin films, we produced a simple rectifier. Rectifiers are semiconductor-based devices that exhibit nonlinear current–voltage characteristics. These devices can be constructed by connecting a semiconductor with two electrodes that have different work functions. Figure 4a shows the current–voltage (I–V) characteristics, as determined by scanning tunneling spectroscopy, for a nanostructured Pt/$Sn_4Se_{10}^{4-}$/surfactant thin film grown on gold. The gold makes up one electrode, and the Pt/Ir STM tip provides the second electrode in the system. The device shows a small leakage current in this sample from -2.0 to $+0.4$ V on the order of nanoamps. There is an order-of-magnitude increase in the current traveling through the system at 0.4 V, the turn-on voltage. Figure 4b shows similar I–V data for a Ni/$Ge_4Se_{10}^{4-}$/surfactant nanostructured thin-film composite. This sample shows a turn-on voltage of -0.5 V. Both samples show large asymmetry, which is expected for rectification. Notably, these two films of different composition also show significantly different turn-on voltages. The difference of almost 1 V between the turn-on voltages in the two samples indicates that the data arises from a real material-based phenomenon and that the electronic properties of these films can be tuned over a large range through changes in the elemental composition.

In summary, in this work we have reported the synthesis of periodic, surfactant-templated thin films of Zintl clusters with nanoscale periodicity and cubic, hexagonal honeycomb, lamellar, and wormlike structures. The thin-film morphology holds several advantages for the design and synthesis of devices that utilize the semiconducting nature of these non-oxide composites. The variety of compositions synthesized not only demonstrates the breadth of the synthetic method, but also provides a means of tailoring the properties of the inorganic semiconducting framework. Moreover, work is currently underway to remove the surfactant from these materials and produce periodic nanoporous semiconductors. Preliminary results suggest that the substrate stabilizes the nanometer-scale architecture of these composites and makes removal of the surfactant without collapse of the inorganic framework possible.[53] We are also working on the incorporation of semiconducting, structure-directing agents into the organic phase, which could make these materials good candidates for device applications such as photovoltaics and ambipolar FETs.[54] The synthesis of thin-film rectifiers based on these materials is the first step toward developing functional devices that can take advantage of the nanoscale periodicity present in these films.

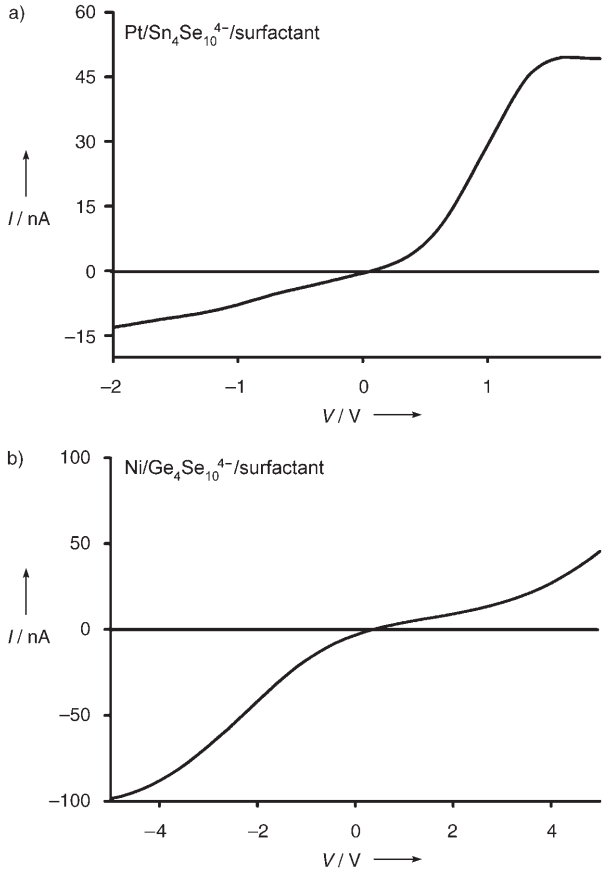

Figure 4. Current–voltage curves for two inorganic/surfactant composite thin film samples as measured by scanning tunneling spectroscopy. a) A Pt/$Sn_4Se_{10}^{4-}$/surfactant nanostructured thin film shows a turn-on voltage of approximately 0.4 V. b) A Ni/$Ge_4Se_{10}^{4-}$/surfactant nanostructured thin film shows a turn-on voltage near -0.5 V. Both curves are asymmetric, which is expected for semiconductor rectifiers. Furthermore, the turn-on voltages vary significantly depending on the composition of the thin film.

Experimental Section

The raw materials for our film growth were prepared by established methods.[55–59] The Zintl clusters ($K_4Ge_4Se_{10}$, $K_4Sn_4Se_{10}$, K_4SnSe_4, K_4SnTe_4) were prepared by direct combination of the constituent elements at high temperature (750 °C) under inert conditions.[55–58]

The surfactant cetyltriethylammonium bromide was prepared by treating triethylamine with 1-bromohexadecane in refluxing ethanol for 3 days.[59] The product was evaporated and then purified by dissolution in chloroform and precipitation with diethyl ether. The white powder was recovered by filtration and then recrystallized from warm acetone.

Non-oxide composite films were synthesized through surface-nucleated growth from a gold substrate. The gold substrates consisted of a glass microscope slide with a thin adherence layer of titanium and a thin layer of gold deposited on the adherence layer. For most composites, the slides were inverted and supported in a synthesis solution consisting of Zintl cluster (0.1 mmol), cetyltriethylammonium bromide (0.3 or 0.6 mmol), and transition metal (0.1 mmol) in formamide (1 mL). For the *Ia3d* cubic phase, these ratios were adjusted slightly to contain Zintl cluster (0.2 mmol), cetyltriethylammonium bromide (0.95 mmol), and transition metal (0.065 mmol) in formamide (1 mL). All of the film mixtures were prepared under an inert atmosphere. The growing films were maintained at 60 °C under inert conditions for 1 h in all cases except for palladium, which was grown for only 25 min to minimize the Pd^{2+} degradation of the gold substrate. After synthesis, the films were washed with copious amounts of formamide under ambient conditions to remove any adhered bulk precipitate. After washing the films in formamide, they were rinsed with acetone and air-dried.

Some Rh-coupled $SnTe_4^{4-}$ thin films were also prepared by using a slightly altered procedure in which $[Rh(en)_x]Cl_3$ was employed as the cross-linking agent. These films were prepared in a similar manner to the method describe above. A solution (0.5 mL) was prepared containing formamide, $SnTe_4^{4-}$, and surfactant. In a second solution, $RhCl_3$ (0.1 mmol) was dissolved in formamide (1 mL) at 60 °C. Ethylenediamine (en; ca. 0.1 mL) was added to the $RhCl_3$ solution. Additional ethylenediamine was subsequently added to the solution dropwise until the color changed from red to colorless. The $[Rh(en)_x]Cl_3$ solution was then added to the Zintl/surfactant solution and placed in an oven at 60 °C for 1 h with a gold-coated substrate. The film was then recovered as described above.

Pure $SnTe_4$ thin films were prepared by using the standard procedure without the addition of a cross-linking transition metal. This Zintl/surfactant solution was mixed and left overnight at room temperature in an inert atmosphere in the presence of a gold-coated substrate. The product was collected the next day and washed with formamide.

The NIR/UV/Vis reflectance data were collected with a Shimadzu UV-3100 spectrophotometer. The reflectance data were measured by utilizing an ISR-3100 integrating sphere attachment because of the optical density of the samples. The collection was made over the wavelength range 2400–200 nm. Low-angle X-ray diffraction (XRD) patterns were collected with a home-built theta-theta powder diffractometer operating with $Cu_{K\alpha}$ radiation.

Scanning tunneling spectroscopy measurements were performed by using a Digital Instruments Nanoscope III in STM mode. After stabilizing a Pt/Ir tip above the sample, the bias of the tip was ramped from −5 to 5 V while holding the tip position constant. In imaging mode, which is used to stabilize the tip position, a bias and current determine the separation. For all scans, the tip position was taken at a bias of 1.135 mV and 100 pA.

Energy-dispersive spectroscopy (EDS) X-ray analysis was carried out on a JEOL TSM-6700F field-emission scanning electron microscope equipped with a liquid-nitrogen-cooled EDAX Super UTW Detector. All elemental spectra were obtained with the scanning electron microscope operating at 25 keV and 20 mA, except that of the platinum composite, which was measured operating at 5–6 keV and 20 mA. All spectra were analyzed with EDAX inc. Genesis Spectrum SEM Quant ZAF Software (version 3.60).

The film thickness was measured by using a Veeco Dektak 6M Profiler. The height of the sample film was assigned as the difference between the height of the film and the height of the bare-gold substrate on which the film was grown.

Received: April 19, 2005
Revised: August 8, 2005
Published online: November 28, 2005

Keywords: nanostructures · self-assembly · surfactants · thin films · Zintl phases

[1] C. T. Kresge, M. E. Leonowicz, W. J. Roth, J. C. Vartulli, J. S. Beck, *Nature* **1992**, *359*, 710.
[2] Q. Huo, D. I. Margolese, U. Clesa, P. Feng, T. E. Gier, P. Sieger, R. Leon, P. M. Petroff, F. Schuth, G. D. Stucky, *Nature* **1994**, *368*, 317.
[3] A. Monnier, F. Schuth, Q. Huo, D. Kumar, D. Margolese, R. S. Maxwell, G. D. Stucky, M. Krishnamurty, P. Petroff, A. Firouzi, M. Janicke, B. F. Chmelka, *Science* **1993**, *261*, 1299.
[4] D. M. Antonelli, J. Y. Ying, *Angew. Chem.* **1996**, *108*, 461; *Angew. Chem. Int. Ed. Engl.* **1996**, *35*, 426.
[5] S. A. Bagshaw, T. J. Pinnavaia, *Angew. Chem.* **1996**, *108*, 1180; *Angew. Chem. Int. Ed. Engl.* **1996**, *35*, 1102.
[6] Z. R. Tian, W. Tong, J.-Y. Wang, N.-G. Duan, V. K. Krishnan, S. L. Suib, *Science* **1997**, *276*, 926.
[7] U. Ciesla, S. Schacht, G. D. Stucky, K. K. Unger, F. Schuth, *Angew. Chem.* **1996**, *108*, 579; *Angew. Chem. Int. Ed. Engl.* **1996**, *35*, 541.
[8] P. Yang, D. Zhao, D. I. Margolese, B. F. Chmelka, G. D. Stucky, *Nature* **1998**, *396*, 152.
[9] M. S. Wong, D. M. Antonelli, J. Y. Ying, *Nanostruct. Mater.* **1997**, *9*, 165.
[10] M. S. Wong, J. Y. Ying, *Chem. Mater.* **1998**, *10*, 2067.
[11] T. Sun, J. Y. Ying, *Angew. Chem.* **1998**, *110*, 690; *Angew. Chem. Int. Ed.* **1998**, *37*, 664.
[12] M. Linden, S. Schunk, F. Schuth in *Mesoporous Molecular Sieves* (Eds.: L. Bonneviot, F. Beland, C. Danumah, S. Giasson, S. Kaliaguine), Elsevier, Amsterdam, **1998**.
[13] G. J. de A. A. Soler-Illia, A. Louis, C. Sanchez, *Chem. Mater.* **2002**, *14*, 750.
[14] L. Pidol, D. Grosso, G. J. A. A. Soler-Illia, E. L. Crepaldi, C. Sanchez, P. A. Albouy, H. Amenitsch, P. Euzen, *J. Mater. Chem.* **2002**, *12*, 557.
[15] E. L. Crepaldi, G. J. de A. A. Soler-Illia, D. Grosso, F. Cagnol, F. Ribot, C. Sanchez, *J. Am. Chem. Soc.* **2003**, *125(32)*, 9770.
[16] D. Grosso, G. J. de A. A. Soler-Illia, E. L. Crepaldi, F. Cagnol, C. Sinturel, A. Bourgeois, A. Brunet-Bruneau, H. Amenitsch, P. A. Albouy, C. Sanchez, *Chem. Mater.* **2003**, *15(24)*, 4562.
[17] D. Grosso, C. Boissiere, B. Smarsly, T. Brezesinski, N. Pinna, P. A. Albouy, H. Amenitsch, M. Antonietti, C. Sanchez, *Nat. Mater.* **2004**, *3*, 787.
[18] H. Yang, A. Kuperman, N. Coombs, S. Mamiche-Afara, G. A. Ozin, *Nature* **1996**, *379*, 703.
[19] H. Yang, N. Coombs, I. Sokolov, G. A. Ozin, *Nature* **1996**, *381*, 589.
[20] C. A. Alberius, K. L. Frindell, R. C. Hayward, E. J. Kramer, G. D. Stucky, B. F. Chmelka, *Chem. Mater.* **2002**, *14*, 3284.
[21] D. Grosso, A. R. Balkenende, P. A. Albouy, M. Lavergne, L. Mazerolles, F. Babonneau, *Mater. Chem.* **2000**, *10*, 2085.
[22] A. Gibaud, D. Grosso, B. Smarsly, A. Baptiste, J. F. Bardeau, F. Babonneau, D. A. Doshi, Z. Chen, C. J. Brinker, C. Sanche, *J. Phys. Chem. B* **2003**, *107*, 6114.
[23] H. Yang, N. Coombs, I. Sokolov, G. A. Ozin, *J. Mater. Chem.* **1997**, *7*, 1285.
[24] T. Nassivera, A. G. Eklund, C. C. Landry, *J. Chromatogr.* **2002**, *973*, 97.
[25] A. Sayari, *Chem. Mater.* **1996**, *8*, 1840.

[26] B. J. Scott, M. H. Bartl, G. Wirnsberger, G. D. Stucky, *J. Phys. Chem. A* **2003**, *107*, 5499.
[27] T.-Q. Nguyen, J. Wu, V. Doan, B. J. Schwartz, S. H. Tolbert, *Science* **2000**, *288*, 652.
[28] A. E. Riley, S. H. Tolbert, *J. Am. Chem. Soc.* **2003**, *125*, 4551.
[29] K. K. Rangan, P. N. Trikalitis, C. Canlas, T. Bakas, D. P. Weliky, M. G. Kanatzidis, *Nano Lett.* **2002**, *2*, 513.
[30] P. N. Trikalitis, K. K. Rangan, M. G. Kanatzidis, *J. Am. Chem. Soc.* **2002**, *124*, 2604.
[31] P. N. Trikalitis, K. K. Rangan, T. Bakas, M. G. Kanatzidis, *Nature* **2001**, *410*, 671.
[32] K. K. Rangan, P. N. Trikalitis, M. G. Kanatzidis, *J. Am. Chem. Soc.* **2000**, *122*, 10230.
[33] M. Wachhold, K. K. Rangan, M. Lei, M. F. Thorpe, S. J. L. Billinge, V. Petkov, J. Heising, M. G. Kanatzidis, *J. Solid State Chem.* **2000**, *152*, 21.
[34] M. J. MacLachlan, N. Coombs, G. A. Ozin, *Nature* **1999**, *397*, 681.
[35] K. K. Rangan, S. J. L. Billinge, V. Petkov, J. Heising, M. G. Kanatzidis, *Chem. Mater.* **1999**, *11*, 2629.
[36] P. N. Trikalitis, K. K. Rangan, T. Bakas, M. G. Kanatzidi, *J. Am. Chem. Soc.* **2002**, *124*, 12255.
[37] S. D. Korlann, A. E. Riley, B. L. Kirsch, B. S. Mun, S. H. Tolbert, *J. Am. Chem. Soc.* **2005**, *127*, 12516.
[38] D. T. Cromer, R. L. Mills, D. Schiferl, L. A. Schwalbe, *Acta Crystallogr. Sect. B* **1981**, *37*, 8.
[39] J. C. Vartuli, K. D. Schmitt, C. T. Kresge, W. J. Roth, M. E. Leonowicz, S. B. McCullen, S. D. Hellring, J. S. Beck, J. L. Schlenker, D. H. Olson, E. W. Sheppard, *Chem. Mater.* **1994**, *6*, 2317.
[40] J. E. Gordon, *The Organic Chemistry of Electrolyte Solutions*, New York, Wiley, **1975**.
[41] D. F. Evans, D. D. Miller, *Water Sci. Rev.* **1989**, *4*, 1.
[42] I. A. Aksay, M. Trau, S. Manne, I. Honma, N. Yao, L. Zhou, P. Fenter, P. M. Eisenberger, S. M. Gruner, *Science* **1996**, *273*, 892.
[43] S. Manne, T. E. Schaeffer, Q. Huo, P. K. Hansma, D. E. Morse, G. D. Stucky, I. A. Aksay, *Langmuir* **1997**, *13*, 6382.
[44] S. Manne, *Prog. Colloid Polym. Sci.* **1997**, *103*, 226.
[45] $Pd^{2+} \rightarrow Pd^{0}$ 0.92 V, $Au^{3+} \rightarrow Au^{0}$ 1.36 V, $Ti^{2+} \rightarrow Ti^{0}$ −1.63 V; from: D. F. Shriver, P. Atkins, C. H. Langford, *Inorganic Chemistry*, 2nd ed., W. H. Freeman, New York, **1994**.
[46] A. E. Riley, S. H. Tolbert, *Res. Chem. Intermed.*, in press.
[47] J. C. Huffman, J. P. Haushalter, A. M. Umarji, G. K. Shenoy, R. C. Haushalter, *Inorg. Chem.* **1984**, *23*, 2312.
[48] J. Tauc, R. Grigorovici, A. Vancu, *Phys. Status Solidi* **1966**, *15*, 627.
[49] A. Rantzer, H. Arwin, J. Birch, B. Hjorvarsson, J. W. P. Bakker, K. Jarrendahl, *Thin Solid Films* **2001**, *394*, 256.
[50] R. M. Mehra, S. Kohli, A. Pundir, V. K. Sachdev, P. C. Mathur, *J. Appl. Phys.* **1997**, *87*, 7842.
[51] T. Gomi, Y. Hirose, T. Kurosu, T. Shiraishi, M. Iida, Y. Gekka, A. Kunioka, *J. Non-Cryst. Solids* **1980**, *41*, 37.
[52] I. Lefebvre, M. A. Szymanski, J. Olivier-Fourcade, J. C. Jumas, *Phys. Rev. B* **1998**, *58*, 1896.
[53] S. D. Korlann, S. H. Tolbert, unpublished results.
[54] A. P-Z. Clark, K.-F. Shen, Y. F. Rubin, S. H. Tolbert, *Nano Lett.* **2005**, *5*, 1647.
[55] O. Palchik, A. Gedanken, V. Plachik, M. A. Slifkin, A. M. Weiss, *J. Solid State Chem.* **2002**, *165*, 125.
[56] J. C. Hauffman, J. P. Haushalter, A. M. Umarji, G. K. Shenoy, R. C. Haushalter, *Inorg. Chem.* **1984**, *23*, 2312.
[57] A. M. Pirani, H. P. A. Mercier, D. A. Dixon, H. Bormann, G. J. Schrobligen, *Inorg. Chem.* **2001**, *40*, 4823.
[58] K. O. Klepp, F. Fabian, *Z. Naturforsch. B* **1999**, *54*, 1499.
[59] F. M. Menger, C. A. Littau, *J. Am. Chem. Soc.* **1993**, *115*, 10083.

